

Initial Properties of Steady State RF Plasma Source by Two Turn Flat Loop Antenna for DEMO Relevant Divertor Simulation Experiment^{*)}

Takumi SETO, Naomichi EZUMI, Reina MIYAUCHI, Naoki SHIGEMATSU, Takuma OKAMOTO, Satoshi TAKAHASHI, Kosuke TAKANASHI, Mafumi HIRATA, Satoshi TOGO, Mizuki SAKAMOTO, Takeru FURUKAWA¹⁾ and Shunjiro SHINOHARA²⁾

Plasma Research Center, University of Tsukuba, Tsukuba, Ibaraki 305-8577, Japan

¹⁾*Kobe University, Kobe, Hyogo 657-8501, Japan*

²⁾*Tokyo University of Agriculture and Technology, Koganei, Tokyo 184-8588, Japan*

(Received 9 January 2023 / Accepted 15 March 2023)

To study DEMO divertors, some linear devices have attempted to create DEMO-grade high-density steady-state divertor simulation plasma in a stronger magnetic field. Helicon plasma sources using a flat-type antenna, which are one of the methods of radio frequency (RF) plasma generation in magnetic field, are expected to achieve this. In this study, we developed a new RF plasma source with a two-turn flat-loop antenna with RF sources having a maximum output power of 30 kW in continuous waves. A two-turn flat-loop antenna is expected to have a large-diameter discharge, and its radial density profile can be controlled. In addition, a water-cooled, double-disc quartz window unit was installed for a high-density, high-power discharge. In the initial experiment, argon and hydrogen plasmas were generated, and the integrity of the new device up to 5 kW, was confirmed in a discharge experiment. The magnetic field conditions were changed in this experiment, and a mode change from capacitively coupled plasma (CCP) to inductively coupled plasma (ICP) during argon discharge was observed. Under the experimental conditions of this study, neither argon nor hydrogen produced helicon plasma. This study hereby, discusses the plasma characteristics and provides guidelines for future development.

© 2023 The Japan Society of Plasma Science and Nuclear Fusion Research

Keywords: divertor, linear device, plasma source, RF plasma, helicon plasma, argon, hydrogen

DOI: 10.1585/pfr.18.2401054

1. Introduction

In order to realize DEMO and future fusion reactors, it is critical to reduce the heat load to the divertor. Currently, divertor simulation experiments are being conducted using many linear devices to investigate the physics of detachment plasma, which is one of the methods used to reduce the heat load [1–5]. In typical linear devices, the electron density n_e and temperature T_e are $\sim 10^{19} \text{ m}^{-3}$ and $\sim 10 \text{ eV}$, respectively. Hence, these devices simulate the detached plasma near a divertor plate [1]. In order to investigate detachment plasma in a more relevant plasma condition, which is expected in the entire scrape-off layer (SOL) and divertor region in DEMO, higher electron densities of approximately about $10^{20} - 10^{21} \text{ m}^{-3}$ and electron and ion temperatures above 100 eV in the steady state, are required [1]. In addition, a large plasma diameter under a strong magnetic field is expected in a real-scale DEMO-grade divertor region [6]. However, no linear device satisfies all the conditions of the DEMO-relevant divertor simulation plasma [1, 7]. The pilot GAMMA PDX-SC, which is

a superconducting mirror device, is currently under development at the University of Tsukuba. The pilot GAMMA PDX-SC aims to contribute to the development of an experimental linear device under DEMO divertor conditions. One of the major challenges in the development of the pilot GAMMA PDX-SC is plasma generation at a steady state, with high density and large diameter in strong magnetic fields.

Radio-frequency (RF) plasma sources can generate plasmas with various parameters depending on their external magnetic field and RF power. There are three discharge modes exist: capacitively coupled plasma (CCP), inductivity coupled plasma (ICP) and helicon plasma [8]. Helicon plasma sources can generate steady-state high-density plasmas with a diameter has achieved 74 cm using a flat spiral antenna [8]. These are expected to be advantageous for steady-state, high-density, and large-diameter plasma generation. Additionally, the radial density profile can be controlled by changing the radiation field patterns of the antenna using a flat spiral antenna [9]. However, scientific and technical challenges still need to be overcome. Therefore, a novel helicon plasma source is required to address these issues. In particular, steady-state hydrogen-

author's e-mail: seto_takumi@prc.tsukuba.ac.jp

^{*)} This article is based on the presentation at the 31st International Toki Conference on Plasma and Fusion Research (ITC31).

helicon plasmas with flat antennas have not been investigated sufficiently. In addition, helicon plasmas of light elements, such as hydrogen, are expected to require high-power discharges of several kilowatts, which can cause thermal problems in the equipment [10].

Therefore, in this study, a novel RF plasma source with a two-turn flat-loop antenna is developed. The two-turn flat-loop antenna is of the same type as the flat spiral antenna. In addition, the radiation pattern can be changed to control the radial density profile. In this paper, we report the design and plasma characteristics of a new water-cooled kilowatt-level steady-state discharge device as a first step in the development of a two-turn flat-loop antenna plasma source, and discuss future development strategies and challenges.

2. Experimental Setup

An RF plasma source was installed in a Compact Test Plasma (CTP) device [11]. The CTP had diagnostic and plasma source regions as shown in Fig. 1 (a). A capacitance gauge was installed inside the vacuum vessel in the plasma source region (gas inlet port). In addition, a capacitance gauge and cold cathode gauge were installed in the diagnostic region. An 800 L/s turbo molecular pump maintained a sufficiently low pressure of the order of 10^{-5} Pa. The inlet gas flow rate was controlled using a mass-flow controller.

The diagnostic region had two magnetic field coils and a measurement port at the center. A maximum current of 65 A was applied to the magnetic-field coils. As the magnetic field strength is a critical parameter in helicon plasma generation, in this study, experiments were conducted in two different magnetic fields. Figure 1 (b) shows the magnetic field strength profiles along the z-axis for the 65 A and 25 A magnetic field coils. The radial-line-integrated emission intensities were observed using a spectrometer (AvaSpec-ULS4096CL-EVO-UA-10) placed between the two coils. The spectrometer had a grating of 300 lines/mm, a wavelength range of 350 nm to 800 nm, and line resolution of 0.50 nm to 0.70 nm in the FWHM. The end-plate, which was a 10 cm diameter disc at the end of the device, floated electrically.

A two-turn flat-loop antenna was installed by replacing the original direct-current (DC) arc source. The outer diameters (O.D.) of the inner and outer loops were 5 and 10 cm, respectively. The antenna was made of copper and had a water channel for cooling. In this experiment, the antenna was placed approximately 68 cm from the center of the magnetic coils ($z \approx -68$ cm), and the feeding point was at one end of the outer loop. The outer and inner loops were connected, and the number of modes in the radial direction was zero. An RF power supply, 30 kW, 13.56 MHz continuous wave (CW), and a matching box (MB) with a split tank circuit were placed in the plasma source region. The RF wave emitted from the antenna propagated into the

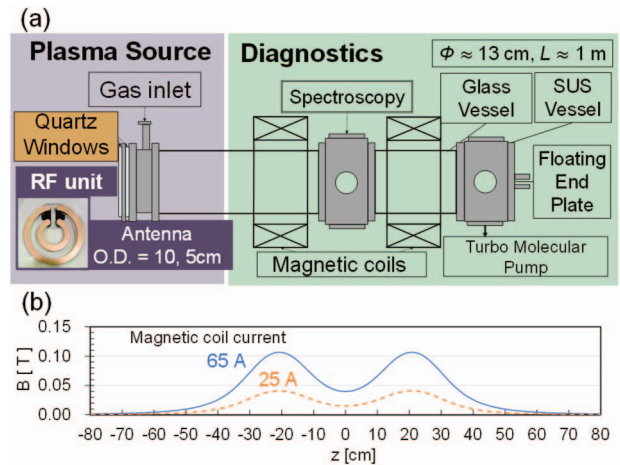


Fig. 1 (a) Schematic diagram of the CTP and (b) magnetic field strength profiles on the z-axis of the CTP.

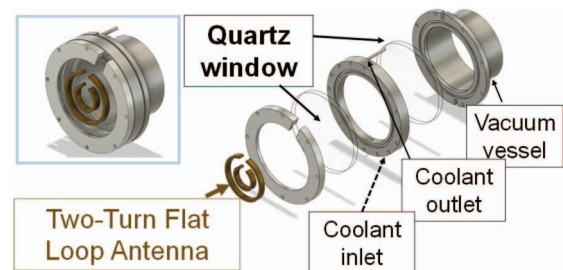


Fig. 2 Schematic diagram of a water-cooled, double disc quartz window unit.

vacuum vessel through a pair of quartz windows to generate plasma. Figure 2 shows the water-cooled double-disc quartz window unit. Water was circulated between the two quartz windows, cooling them evenly. This allowed RF penetration into the vacuum vessel and protected the windows from heat from the plasma and RF antenna. Although conventional helicon plasma sources with water-cooled window [10], our system is the first example of a flat-type antenna with a fully water-cooled window.

3. Results and Discussions

The RF discharges started with 190 W of RF power input for argon (Ar). Hydrogen plasma generation began at less than 500 W. The newly introduced RF circuit and water-cooled double-disc quartz window unit functioned effectively. The temperature change in the quartz windows was within the acceptable range of less than 5 kW. However, during input RF power of almost 5 kW, the vacuum vessel close to the discharge region reached approximately 60°C. In addition, abnormal discharges were observed, indicating discharges outside the vacuum vessel, such as discharges in the matching box, depending on the experimental conditions.

3.1 Argon plasma generation

Figure 3 shows the Ar plasma generated under the conditions of coil current 65 A, input RF power 2 kW, and gas pressure of 0.3 Pa in the diagnostics region. Plasma is confirmed to be present throughout the vacuum vessel. Figure 4 shows the floating potential measured using the end plate. When the RF power is almost 2 kW at 25 A, the floating potential (V_f) changes nonmonotonically, suggesting that the discharge mode changes. At 65 A, V_f changes continuously to 3.5 kW. The power is further increased, and an abnormal discharge occurs in the MB.

Figure 5 shows the emission spectra before and after the mode change. The ArI emission at approximately 750 nm is stronger than that at approximately 400 nm. Here, we discuss whether the observed mode is ICP or helicon. The helicon mode is characterized by a very high electron density and bright ion emission in the radially localized central core region, known as the blue core [12]. However, such strong ion emission (ArII) is not observed. Therefore, based on these results, we can conclude that the observed mode change is due to ICP.

To further evaluate the relative electron density, we focus on the emission intensity. The ArII emission intensity I_{ArII} can be written as follows, assuming that the plasmas are quasi-neutral, and the electron temperature is constant [13].

$$I_{\text{ArII}} \propto n_e^2, \quad (1)$$

where n_e denotes the electron density. Figure 6 shows the RF power dependence of $\sqrt{I_{\text{ArII}}}$, which is proportional to n_e (Eq (1)), using the wavelength 420.1556 nm and the emission from $5s^4P$ to $4p^4D^{\circ}$. The assumption of a constant electron temperature can then, be made by considering the following. The floating potential depends on the space potential and electron temperature, and as the floating potential is almost constant up to 2 kW (in Fig. 4), it can be considered that the electron temperature is almost constant if the space potential is constant. In these experiments, plasmas were generated in the entire vacuum vessel (see Fig. 3), and the electron loss to the vessel walls related to the space potential was less affected by the power rise. Therefore, the space potential can be assumed to be almost constant. As shown in Fig. 6, at 65 A, n_e is slightly higher owing to the stronger magnetic field. In both cases of 65 A and 25 A, before the mode change, n_e increases as the input power increases. It may be noted that the comparison of n_e between the plasmas before and after the mode change is not appropriate because the electron temperature changes as the floating potential changes at 2 kW in the case of 25 A.

3.2 Hydrogen plasma generation

Hydrogen plasmas were generated at the magnetic coil currents of 25 A and 65 A, a gas pressure of 0.2 Pa in the diagnostic region, and an input RF power of up to 4.5 kW. Figure 7(a) shows the emission intensity ratio of

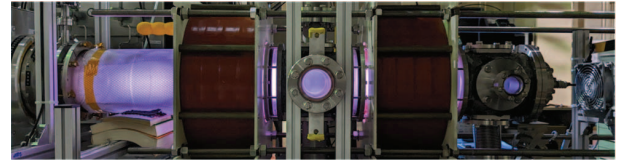


Fig. 3 Argon plasma generation experiment in CTP; the magnetic coil current is 65 A, gas pressure at the diagnostics region is 0.3 Pa and the input RF power is 2 kW.

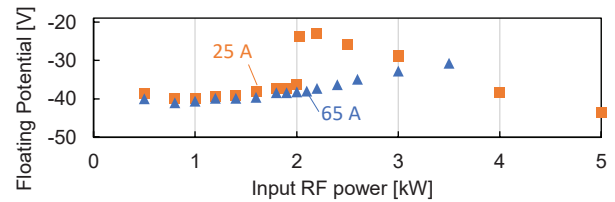


Fig. 4 Power dependence of the floating potential at the end plate when the magnetic coil current is 25 A (orange closed squares) and 65 A (blue closed triangles).

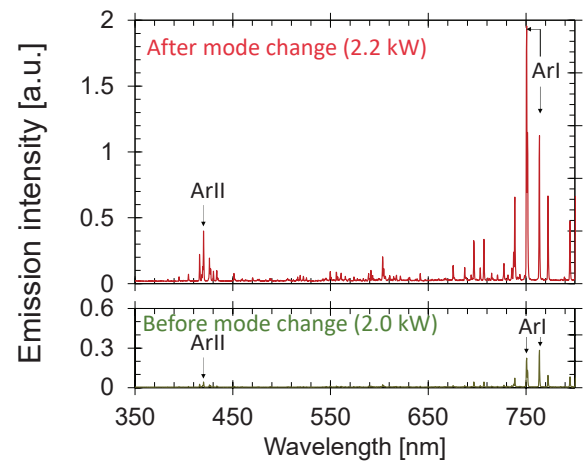


Fig. 5 Emission spectrum of an Ar plasma in the CTP with magnetic coil current 25 A when the input RF power is 2.2 kW (red line) and 2.0 kW (green line).

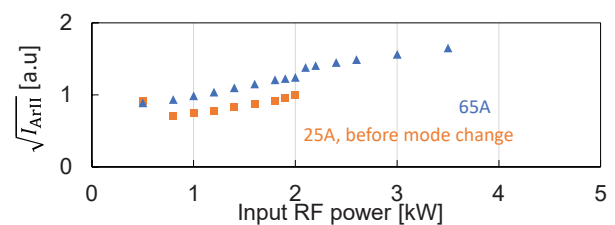


Fig. 6 Power dependence of the square root emission intensity of Ar II (420.1556 nm) which is proportional to n_e when T_e is constant [13].

the Fulcher-band ($d^3\Pi_u - a^3\Sigma_g^+$) to H_α , $I_{\text{Fulcher}}/I_{H\alpha}$. For I_{Fulcher} , the total intensity of the transition of the rovibrational state $v = 1$ to 1 in the Q branch $j = 1, 2, \text{ and } 3$ is

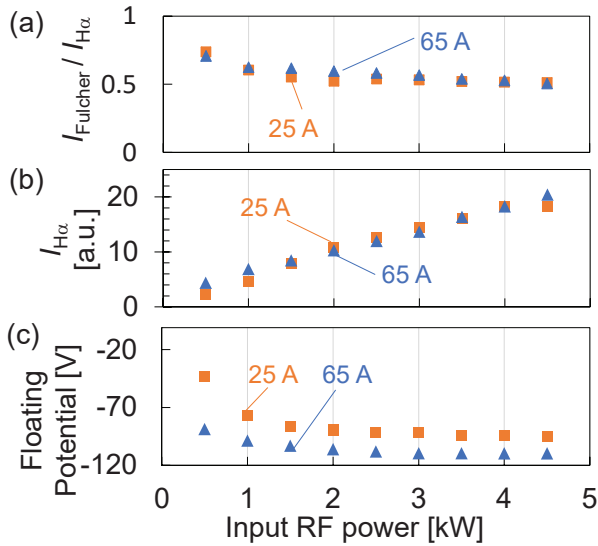


Fig. 7 Power dependence of (a) emission intensity ratio of one of the Fulcher- α band lines to H_{α} , (b) emission intensity of H_{α} , and (c) floating potential at the end plate on CTP at 0.2 Pa, magnetic coil current 25 A (orange) and 65 A (blue).

used. $I_{\text{Fulcher}}/I_{\text{H}\alpha}$ is almost constant with the input power, with a maximum ratio of 0.73 and a minimum ratio of 0.53. For incident powers greater than 1 kW, the ratio remains almost constant. No differences are evident in the ratio with respect to the magnetic field strength. Reference [14] described $I_{\text{H}\alpha}$; I_{Fulcher} as

$$I_{\text{H}\alpha} \propto n_e n_{\text{H}_2} \langle \sigma v \rangle_{\text{dis}, \text{H}(n=3)}, \quad (2)$$

$$I_{\text{Fulcher}} \propto n_e n_{\text{H}_2} \langle \sigma v \rangle_{\text{ex}, \text{H}_2(d^3\Pi_u)}, \quad (3)$$

where, $\langle \sigma v \rangle$ are the rate coefficients derived from the cross sections by averaging the Maxwellian distribution function. $\langle \sigma v \rangle_{\text{dis}, \text{H}(n=3)}$ is the dissociative excitation of electron collision and $\langle \sigma v \rangle_{\text{ex}, \text{H}_2(d^3\Pi_u)}$ is direct excitation from electron excitation. The ratio of $I_{\text{Fulcher}}/I_{\text{H}\alpha}$ is a function of the rate coefficients only, which are a function of the electron temperature [14]. According to [14], it is suggested that the electron temperature is between several eV in this case. The power dependence of the electron temperature is also considered to be almost constant for incident powers greater than 1 kW. It may be noted that in [14], similar experimental conditions were used, including low gas pressure (up to 0.27 Pa), low electron density ($\sim 10^{16} \text{ m}^{-3}$), but electron cyclotron resonance plasma generation.

Figure 7 (b) shows the power dependence of $I_{\text{H}\alpha}$. Its value increases by one order of magnitude. According to Eq (2), $I_{\text{H}\alpha}$ can be increased through three terms, electron density n_e , hydrogen molecule density n_{H_2} and the rate coefficient of dissociative excitation. Although n_{H_2} can increase due to the recycling of hydrogen absorbed in the vacuum vessel wall, its contribution is considered to be very small in this case. When the input RF power is greater than 1 kW, the rate coefficient is almost constant because

the T_e is almost constant in this region. Therefore, we conclude that an increase in $I_{\text{H}\alpha}$ is strongly influenced by an increase in n_e . However, because of the strong temperature dependence of the reaction rate coefficient in the region of a few electron volts [15], detailed electron temperature measurements are required to develop this discussion.

The abovementioned results show almost no difference for magnetic coil currents of 25 A and 65 A. However, the floating potential at 65 A is slightly deeper than that at 25 A (shown in Fig. 7 (c)), which is attributed to the suppression of electron loss to the wall caused by the increase in the magnetic field. This consideration is driven by the evaluation of the radial diffusion coefficients of electrons and ions. We expect this to be an important guideline for magnetic field strength design in plasma source development, and one of the most important issues to be addressed in the future.

In this study, we did not consider reactions involving high-state hydrogen during dissociation and excitation. We considered models that accounted for these reactions (the collisional radiative (CR) model). In the future, we will attempt to optimize the magnetic field strength, configuration, and gas pressure to realize helicon discharge.

4. Conclusion

This study presents the details of the development of a steady-state, high-density, large-diameter plasma source for the pilot GAMMA PDX-SC. A helicon wave plasma source with a flat antenna was developed. A high-power discharge circuit and cooling system were installed. In the discharge test at the CTP, argon and hydrogen plasmas were successfully generated.

In the case of argon, the electron density n_e increases slowly with increasing power. For a further increase in the electron density, a transition to the ICP mode is effective. However, when the magnetic field coil current is 65 A, ICP is not generated. A possible reason is that the electron density is slightly higher than that at 25 A, and the skin depth is slightly shallow, which is an important parameter in ICP. Therefore, it is necessary to measure the absolute value of the electron density. In the case of hydrogen, T_e is almost constant above 1 kW, and it tends to increase with increasing input RF power, according to the emission intensity results. However, the floating potential differs depending on the magnetic field strength, and we infer that the difference is caused by the diffusion coefficient in the radial direction. The diagnosis of T_e and T_i is a future challenge for further discussion of diffusion coefficients.

In the future, we will evaluate the cooling in the RF circuit in detail to further improve the performance and stabilize the circuit. A detailed evaluation of the water-cooled quartz window unit will also be conducted. In addition, we will improve the direct probe measurements for both argon and hydrogen. For helicon plasma generation,

we will perform a detailed search for ICP transition conditions and investigate the magnetic field strength and gas pressure. Such plasma source development will contribute not only to DEMO divertor development but also to applied applications and understanding of RF plasma physics.

Acknowledgments

This work is performed with the support and under the auspices of the NIFS Collaboration Research program (NIFS17KOAF005, and NIFS20KUGM148).

- [1] N. Ohno, Plasma Phys. Control. Fusion **59**, 034007 (2017).
- [2] M. Sakamoto *et al.*, Nucl. Mat. Energy **12**, 1004 (2017).
- [3] N. Ezumi *et al.*, Nucl. Fusion **59**, 066030 (2019).
- [4] E.M. Hollmann, A. Yu. Pigarov and Z. Yan, J. Nucl. Mater **363-365**, 359 (2007).
- [5] R. Perillo *et al.*, Phys. Plasmas **26**, 102502 (2019).
- [6] N. Asakura *et al.*, Nucl. Fusion **61**, 126057 (2021).
- [7] K. Okano *et al.*, Fusion Eng. Des. **136**, 183 (2018).
- [8] S. Shinohara, Adv. Phys. **3**, 1420424 (2018).
- [9] S. Shinohara and T. Tanikawa, Rev. Sci. Instrum. **75**, 1941 (2004).
- [10] S.C. Thakur *et al.*, Plasma Sources Sci. Technol. **30**, 055014 (2021).
- [11] N. Ezumi, Contrib. Plasma Phys. **48**, 5 (2008).
- [12] S.C. Thakur *et al.*, IEEE Trans. Plasma Sci. **43**, 2754 (2015).
- [13] S. Waseda *et al.*, Plasma Fusion Res. **9**, 3406125 (2013).
- [14] K. Kondo *et al.*, J. Appl. Phys. **27**, 1560 (1988).
- [15] B.P. Lavrov and A.V. Pipa, Opt. Spectrosc. **92**, 655 (2002).